EUROPEAN ORGANIZATION FOR NUCLEAR RESEARCH

CERN-EP/86-59
May 22nd, 1986

THE OPAL JET CHAMBER FULL SCALE PROTOTYPE

H.M. Fischer, M. Hauschild, H. Hartmann, A. Hegerath
Physikalisches Institut, Universität Bonn

H. Boerner, H.J. Burckhart, M. Dittmar, R. Hammarström, R.D. Heuer, L. Mazzone, A. Michelini, Ö. Runolfsson, D. Schaile, M. Uldry, S. Weisz, P. Wicht, K. Zankel
CERN, Geneva

R. Kolpin, J. Ludwig, W. Mohr, F. Röhner, H. Röser, K. Runge, O. Schaile, J. Schwarz, H.E. Stier, A. Weltin
Fakultät für Physik, Universität Freiburg

P. Bock, J. Heintze, P. Igo-Kemenes, P. Lennert, R. Rusniak, P. von Walter, A. Wagner, J. Zimmer
Physikalisches Institut, Universität Heidelberg

ABSTRACT

The concept of a jet chamber for the central detector of OPAL has been tested with a full scale prototype. The design of this prototype, its mechanical and electrical structure and its support system for high voltage, gas, laser calibration and readout are described. The operating experience gathered since the summer of 1984 and the chamber performance as measured by its spatial resolution and ability to identify particles are also given.

Presented at the 4th Vienna Wire Chamber Conference
February 1986

INTRODUCTION

The main tracking device of the OPAL detector at LEP will be a large cylindrical jet chamber [1]. The principles of construction and operation of such a device have first been established with the jet chamber of the JADE experiment at PETRA [2]. Since the size of the OPAL chamber is about a factor of two larger in length and radius, a full scale prototype has been constructed to prove the feasibility of the design, to check that the attempted resolution can be reached, to optimize the operating point, and to identify and eliminate possible sources of systematic errors.

The prototype was, therefore, designed to resemble as closely as possible the final jet chamber, especially for critical components like the wire suspension, the shaping of the drift field, and the insulation of the high voltage. The prototype also played an important role in establishing and testing of the manufacturing procedures. As planned for the final chamber, a system of laser beams was part of the full scale prototype to study the feasibility of laser calibration in a big chamber system.

In this report first the design and construction of the various chamber components is presented. Then the high voltage and the gas system, the readout electronics and the laser system for calibration are described. In the last chapter a short summary is given of the various test measurements which have been performed using the full scale prototype. The operating experience is discussed and results are presented on the spatial resolution and on particle identification through multiple sampling of the ionization loss (dE/dx).

1. DESIGN AND CONSTRUCTION OF THE CHAMBER

1.1 Drift cell geometry

The jet chamber of OPAL is of cylindrical shape, the active volume having a total length of about 4 meters and extending in the radial direction from 25 cm to 185 cm. Around the axis of the cylinder which

coincides with the beam direction space is left free for the beam pipe and a special vertex tracking chamber. All wires are stretched between two end plates and run parallel to the axis.

In order to keep multiple scattering and the rate of secondary interactions as low as possible, the jet chamber will be built without an inner support cylinder. The end plates will be held apart only by a shell of 24 aluminium panels located at the outer radius of the cylinder. To minimize the bending of the end plates under the force of the wires of 14 tons, these plates are given a conical shape with a cone angle of 15 degrees. As a consequence the wire length decreases from 4 m at a radius of 185 cm to 3.2 m at 25 cm. The maximum bending of the end plates, made from aluminium of 30 mm thickness and a reinforcement ring at the outer rim, can thus be kept below 1 mm.

The chamber will be mounted inside a pressure vessel where the beam pipe serves as the inner wall of the tank.

Fig. 1 shows a schematic drawing of the chamber. The sensitive volume consists of 24 identical sectors and, in contrast to the JADE chamber, has no subdivision in the radial direction. This design was chosen in order to maximize the track length within the sensitive volume and to minimize areas of possible field distortions. Each sector consists of an anode plane with 160 sense wires and two cathode planes which form the boundaries between two adjacent sectors. All wire planes are oriented in the radial direction.

Since the sectors extend over the full radius of the chamber, the maximum drift distance varies from 3 cm up to 25 cm. Even for the longest drift distance a good timing resolution can be reached by operating the chamber at an elevated pressure [3] and by using a Flash ADC read out system. In the drift region, a homogenous electrical field with equipotential lines parallel to the anode plane is required for accurate position measurement. There is only a small region of the field around the sense wires that has cylindrical symmetry. In order to reduce the sensitivity to field distortions the chamber is operated at the maximum of

the drift velocity curve. For the gas mixture presently used (Argon 88%, Methane 9.4%, Isobutane 2.6%) the maximum of the drift velocity is at 235 V/cm/bar, hence at 4 bar pressure a field of 940 V/cm is required. This leads to an operating voltage of about -27kV at the outer end of the sector. With such high voltages special attention must be paid to the insulation and field shaping at the boundaries of the sector.

The cathode planes are formed by wires and inclined by 7.5° with respect to the equipotential planes. At the outer radius each sector is closed by the so-called barrel field shaping electrode, an insulator covered with copper strips. On the end plates, the endcap field shaping electrodes, which are also insulators with strip electrodes, provide the correct termination of the electrical field. At the inner radius the chamber is equipped with a field cage made of wires and a field shaping foil which is mounted on the vertex chamber support tube.

For the full scale prototype (from now on abbreviated as FSP) two sectors of full dimensions have been built, consisting of two anode and three cathode planes. Wires of 4 m length are strung between the end plates, which are not conical but flat in order to simplify the construction. They are held apart by an aluminium frame with four supporting beams, which allow easy access to the chamber volume. Fig. 2 shows the mechanical structure of the FSP.

1.2 Anode plane

A schematic drawing of the drift cell is shown in Fig. 3. The anode plane consists of 160 equally spaced sense wires, interleaved with potential wires. The distance between adjacent sense wires is 10 mm. As shown in Fig. 3 the sense wires are staggered by 100 μm alternating to the left and right side of the wire plane as defined by the potential wires. This mechanical staggering is further increased to 200 μm by the electrostatic forces. With the help of this staggering of the sense wires the left-right ambiguity of tracks can be resolved using just a wire triplet. The anode wires are at ground potential, the voltage applied to the potential wires (about -2.5 kV) is used to adjust the gas amplification.

The sense wires are gold-plated tungsten-rhenium wires with 25 μm diameter at a tension of 105 grams, which is still well below the elastic limit. The potential wires, made of copper-beryllium alloy are 100 μm thick, and are strung at a tension of 760 grams. Materials and tensions of the wires were selected in tests with an 8-wire prototype chamber, which was also used to establish the electrostatic stability of the 4 meter long wire structure [4]. The wire tensions are chosen such that the gravitational sag (200 μm) is equal for sense wires and potential wires. To reduce the surface fields and the deflections due to the electrostatic forces, the first and last sense wire of each anode plane is 30 μm, the first and last potential wire 175 μm thick. These wires are stretched with higher tensions. One additional wire of 175 μm diameter terminates the anode plane at each end and is held at a potential which is separately adjustable in order to minimize field distortions.

The mounting scheme of the sense and potential wires at the end plates is shown in Fig. 4. The wires run through slots between the field shaping electrodes and then through holes in the end plates. The wires are precisely positioned at the outside of the end plates with the help of an accurately machined comb-like structure carrying V-shaped grooves. In this way the structure which defines the mechanical precision of the chamber is easily accessible and can be surveyed. The comb is made of profiles of dolomite-loaded epoxy resin which are glued onto a 1.6 m long aluminium ruler. Before installation the four rulers used in the FSP were measured and the staggering of the grooves was found to be correct with a RMS deviation of 10 μm. Behind the comb the wires are soldered onto printed circuit boards equipped with solder pads and pins. The boards have slits between the solder pads of the sense and the potential wires to reduce surface leakage currents. The total leakage current per group of 16 wires was typically less than 5 nA. No noise generated on the boards has been observed. The boards carry a high voltage bus for the supply of the potential wires and the resistors and capacitors for the wire termination. This method of wire positioning is described in [4].

The potential wires traverse the end plates in thin copper-beryllium tubes, insulated on the outside with teflon. The tubes are kept at the same voltage as the potential wires, since otherwise a glow discharge or sparking could occur between the wires and the end plates.

1.3 Cathode plane and field shaping electrodes

The cathode planes are made of copper-beryllium wires of 100 μm diameter with a spacing of 3.3 mm. For the final chamber 125 μm thick wires will be used in order to reduce the surface field to well below the critical value of 20 kV/cm. Since the equipotential lines in the drift region are parallel to the anode plane which is inclined by 7.5 degrees with respect to the cathode plane, each wire of the cathode plane is at a different potential. The voltages range from -27 kV at the outer radius to -5 kV at the inner radius. Because of these high voltages the cathode wires cannot be mounted to the end plates in the same way as the sense and potential wires.

A special structure has therefore been designed which supports the cathode wires, correctly shapes the field in the region of the end plates and acts as a high voltage degrader and insulator between the chamber and the end plates. Furthermore it provides an electrically safe encasing for the resistors of the voltage divider chain which supplies the cathode wires and the field shaping electrodes with the correct voltages. A cut away picture of this structure is shown in Fig. 5. The front part, which is directed towards the drift volume, consists of a PC board (FR-4) with the field electrodes and the wire supporting structure with the resistor chain. The PC board is covered with a pattern of 89 copper strips running parallel to the direction of the anode plane (see Fig. 3). The wires are fed through holes onto a small printed circuit board where they are soldered and secured by being wound around pins. The positioning is achieved with a comb-like structure. The resistors of the divider chain are placed on the board and connected directly to the wires. In this way, they are separated from the actual drift volume.

The back part of the structure insulates the end plate from the high voltage. In the final detector to achieve a reliable degradation of 30 kV across an insulator of only 6 mm thickness this part will be a 5 layer structure. Each layer will consist of a 1.2 mm thick FR-4 plate and a copper foil which is held at an appropriate intermediate potential. In the FSP this element is made of a single 6 mm thick FR-4 U-shape profile covered with the same copper strip pattern as the front part. The pattern is shifted by one strip width to provide a better shielding against ground. An aluminium profile is glued to the back of the field degrader. This profile is attached to the endplate by bolts.

Connections to the voltage divider chain are provided at five points : at the top and bottom end of the chain and at three intermediate points. So far only the top and the bottom point of the chain have been supplied with voltage the others have only been used for monitoring purposes. At high rates it might become neccessary to connect also the three intermediate points in order to maintain the correct potential drop along the chain.

The field shaping at the inner radius of each sector is done with wires. The appropriate voltages are supplied by an additional resistor chain. At its outer radius each end cap field shaping electrode is attached to the barrel field shaping electrode through card edge connectors. In this way the barrel electrodes receive their voltages from the endcap electrodes, so they do not need additional resistor chains. A further benefit is the direct interconnection between the cathode wires and the barrel and endcap electrodes. In this way the electrodes act as damping capacitors for the cathodes, eliminating crosstalk between sectors.

At the place where the barrel electrode is connected to the end cap electrode, both structures overlap for about 15 cm in order to achieve the proper termination of the electric field. To save space the barrel electrode is bent around the end cap electrode.

The barrel field shaping electrodes which are 4 m long and 0.48 m wide are made from rectangular FR-4 plates of 6 mm thickness. Two pieces of 2 m each have been glued together. The surface facing the drift volume carries 179 copper strips of 1.3 mm width with a pitch of 2.7 mm. Under normal operating conditions the voltage drop between strips is about 250 volts. The barrel field electrodes are mounted directly onto the aluminium panels which close the drift chamber at the outer radius.

The FSP contains two active anode planes and three cathode planes. In order to properly terminate the electric structure the next anode plane on each side is simulated by a large copper clad FR-4 plate, inserted at the appropriate position. These planes are put on -2 kV, the mean potential of an anode plane, thereby symmetrizing the electric fields.

1.4 Assembly and wire stringing

The end plates were first mounted to the support beams and aligned, then two anode planes were strung between them. Anode and potential wires were given the proper tension by a simple pulley and weight system. The wires were soldered onto the pad of the suspension which was nearest to the comb. They were wound around pins to secure them and soldered again to both the pins and a second solder pad. A special solder containing silver was used to prevent the dissolving of the gold coating on the sense wires [5]. The tension of each wire was checked by measuring the resonance frequency [6]. A maximum deviation of 7 μm from the nominal sagitta value was allowed. The observed variations were due to changes in the wire diameter, which was confirmed independently with an electron microscope. The correction was made by adjusting the weights accordingly.

The positioning accuracy achieved for the sense wires in the anode planes was checked optically with a level. Fig. 6 shows the relative positions of the wires. The distributions have a spread of less than 10 μm, which is much less than the spatial resolution of the chamber.

The cathodes were strung separately on a table where a clamping mechanism held the front part of the endcap field electrodes at the same

distance as in the final position between the endplates. Then the wires were inserted using the procedure described for the anode plane. They were also checked for proper tension. After completion of a plane, the tension was released and the back parts of the electrodes were mounted. The field electrodes together with the cathode wires were then transfered to a mounting jig, which was used to insert the plane into the space between the endplates. The aluminium profiles of the endcap degrader were fixed to the endplates with bolts and the tension was gradually reapplied.

The influence of the accuracy in the relative positions of the anode and cathode planes was studied using electrostatic calculations. To maintain a gas gain variation of less than one percent the distance between the anode and cathode planes must have a relative accuracy of 1×10^{-3}. Depending on the radius this requires an absolute precision of 40 to 300 μm, which can readily be achieved. The homogeneity of the drift velocity is a less demanding requirement since to maintain its uniformity to 1×10^{-4} within one sector the accuracy in the relative position between planes need only be 1×10^{-2}.

All critical positioning of the anode combs and of the cathode planes is done with the help of precisely machined holes and dowel pins. No adjustment is forseen after assembly.

2. HIGH VOLTAGE SYSTEM

The high voltage system (Fig. 7) has to supply to the cathode resistor chains voltages of up to -27 kV at the top feed point and -5 kV at the bottom feed point. Each cathode plane is fed via two resistor chains, one on each end of the wire plane. The potential wires require a voltage around -2.5 kV, depending on the gas amplification desired. The stability requirements are very high : to keep variations of the amplification below 1%, the potential voltage has to be stable to 1 volt and the cathode voltage to 5 volts. All 3 cathode planes with a total of 6 resistor chains are connected to the same power supplies to guarantee

the same voltages throughout the chamber. For diagnostics purposes and for safety reasons the currents into the resistor chains are monitored separately for each cathode.

For the same reasons all potential wires of one sector are supplied by one power supply, but the currents in the chamber are monitored per group of 16 wires. Typical values for the potential currents are 5 nA per group. The safety system has an emergency threshold set at 10 μA. If this limit is reached the potential wire voltages are connected to ground within 1 μs by transistor switches. All other voltages are cut off more slowly by HV relays.

For adjusting the voltages a master/slave system is used. The voltages can be set directly by the slave control, whereas the master ramps all voltages proportionally according to the slave settings. This scheme is very useful for testing the chamber by applying only a small percentage of the final voltages. For a smooth turn-on an automatic ramping with a nonlinear speed/time curve is used. Inside the pressure tank each incoming HV cable is passed through a low pass filter to block RF noise.

3. GAS SYSTEM

Gas properties like drift velocity and electron attachment have to be kept stable over a period of several months in the presence of outgasing from detector materials. The stability is dictated by the spatial and charge resolution that is required. The gas mixture used so far in the operation of the FSP has been the one used in the JADE detector (Argon 88%, Methane 9.4% and Isobutane 2.6%). The gas system (Fig. 8) has therefore to provide a 3-component gas mixture at a pressure of up to 4 bar. It has to eliminate oxygen from the gas with high efficiency down to a level of a few ppm, since oxygen has a large effect on electron attachment.

Before filling the chamber with gas, the whole system, which has a volume of 30 m^3 is pumped down with ROOTS pumps through a cold trap to a final pressure of 10^{-6} bar, where it is kept for at least 24 hours. Then it is filled successively with the three components; the mixture is controlled by partial pressures. The system is then disconnected from the gas supplies. The gas is circulated through a chemical filter of the activated copper type (BASF R311) to remove oxygen. For the initial cleaning of the gas the circulation rate is 60 m^3 per day. Stable conditions are reached after about 10 complete circulations of the gas volume.

Since the presence of water in the gas both reduces rate of radiation damage to the signal wires and modifies the drift velocity [7], its amount must be kept constant and was chosen to be 500 ppm. Two molecular sieves (3 Angstroem) are therefore added in parallel to the gas volume : one to remove water and one, saturated, to release water into the gas by heating.

The control of the gas quality requires sophisticated instrumentation. The oxygen content is measured with a Teledyne trace oxygen analyser which works down to a concentration of 1 ppm. Water concentration is measured with a Shaw hygrometer. The most important instrument is a small test chamber which enables monitoring of the drift velocity, gas amplification and electron attachment. This chamber is described in detail in [8]. During typical periods of one month the gas density was constant to 0.1% and no change in the gas composition due to removal of methane or isobutane was detected. For this reason, no addition of fresh gas was necessary.

4. READOUT SYSTEM

The jet chamber provides three-dimensional coordinates of the particle tracks by measuring the drift-time and by recording the signal charges at both ends of the sense wires. Low noise preamplifiers (VV 36, Table 1) are mounted onto the end plates as close as possible to the anode

fixations. No pulse shaping by pole zero cancellation has been applied. For the first tests with the FSP no hardware cross-talk compensation was used, but it was introduced in one sector for the second beam test in May 1985. For signal transmission, three types of cables have been tested : unshielded, commonly shielded and individually shielded twisted pair cable. The last one was the best choice with respect to attenuation and noise level.

The waveform of the analog signal is recorded with 100 MHz flash analog-to-digital converters (FADCs, Table 2). The FADCs are essential to extract the maximum amount of information from the chamber signals. In particular the time measurement and the double hit resolution are greatly improved by a high speed wave form sampling. The different components of the FADC system (DL300) are described in detail elsewhere [9]. The FADCs have a six bit resolution, which is effectively extended to eight bits by a non-linear response function. Digital data are stored in fast memories 256 samples deep. The memory depth is presently extended to 1024 samples to provide the necessary time range for large drift distances. The digitized information is read out via a hardware scanner, which normally performs a zero suppression to reduce the amount of data. During beam tests the raw event length of 100 kbyte was reduced on the average to about 15 kbytes by this method. Each FADC board carries 4 channels. Each crate, holding a total of 24 boards, is assigned a microprocessor which reads and formats the data and writes them into a memory in a CAMAC crate. From there the data are read into a VAX 11/750. This distributed readout was tested up to a rate of 25 events/sec with 1.5 tracks/event on average.

So far one sector has been equipped with readout electronics. During the last 18 months, there have only been a few failures in the modules. The operational stability of the system has been very good.

5. LASER CALIBRATION SYSTEM

The laser calibration system (Fig. 9) is used to study calibration procedures for position measurements, drift velocity and to test hardware components of the chamber. A frequency quadrupled Nd-Yag laser is used. At the wavelength of 266 nm the photon energy is 4.68 eV, sufficient for two-photon ionization of many aromatic impurities [10] which are present in the chamber gas [11]. So far seeding of the chamber gas was not necessary to obtain good signals.

The beam is passed through a beam expanding telescope with a diaphragm and is then guided by 4 dielectric mirrors into the pressure vessel over a distance of up to 15 meters. The beam profile is nearly gaussian. The beam is focussed by a telescope to a spot size of 1 mm in the chamber. A scanning mirror, mounted at the vertex position, can be rotated in both the polar angle Θ and the azimuthal angle φ by remote control to move the laser beam over the full volume of the FSP. A dielectric beam splitter in front of the scanning mirror provides two parallel beams of 10 mm nominal separation. Separation and parallelism of the two beams have been measured with a photodiode array of 1024 pixels of 15 μm pitch to an accuracy of better than 5 μm corresponding to 1/100 mrad. With a spot size of 1 mm^2 and a pulse duration of 4 nsec pulse energies of 2 to 5 μJ are sufficient to obtain a charge corresponding to a minimum ionizing particle. Over the entire beam length inside the chamber the recorded deposited charge is uniform to 20%.

So far calibration methods relying on the straightness of the laser track have been developed. Methods for measuring the drift velocity with the double beam are under study.

6. RESULTS OF MEASUREMENTS WITH THE FSP

6.1 Test setups

The performance of the FSP has been studied in a test beam and with cosmic rays. For tests with cosmic rays the chamber was mounted on top of a counter telescope consisting of iron blocks interleaved with scintillators.

Muons with $p \geq 500$ MeV or with $p \geq 5$ GeV could be selected by the trigger. This setup was used in a combined test with other chambers of the OPAL central detector and in a search for alternative operating points. In addition a coarse study of the relativistic rise of the specific energy loss has been performed with cosmic rays. For detailed investigations of the dE/dx measurement test beam data were used. The particle separation capabilities of the FSP have been analysed in 1984 and 1985 in a 6 GeV beam containing electrons, pions and protons. The particles were identified independently with Cherenkov counters and by time of flight.

In order to be able to illuminate different regions of the sectors, the chamber was mounted on a support which allowed translations in both direction perpendicular to the beam. In addition the chamber could be rotated around the horizontal axis, which was parallel to the sense wires and around the vertical axis.

During the last 18 months, there have been frequent tests with the laser system, either to study calibration procedures or to address specific questions in connection with tests of components, for example the performance of different preamplifiers. The flexibility and availability of the laser system was very useful for these tests.

6.2 Operating experience

The FSP has been in operation for 18 months. The basic design has been proven to be correct. No component showed design errors or developed reliability problems. In particular the HV-degrading schemes and the laser system were shown to work at full scale. The operational characteristics have been stable throughout the different test periods.

One important effect observed in the FSP is the collective cross-talk, which is due to the fact that each sense wire induces small signals of opposite polarity on its adjacent wires. This causes the timing accuracy to deteriorate and introduces a correlation between adjacent pulse height measurements. The way in which this cross-talk manifests itself depends

on the relative timing of the signals on adjacent wires and therefore on the angle of the track with respect to the anode plane. The influence on the timing accuracy has clearly been observed and is strongest for tracks running parallel to the anode plane, since then real signal and cross-talk signals overlap completely. Using tracks that cross over a cathode plane, the cross-talk charge at the first neighbour was measured to be about 8% of the actual signal. At the second neighbour it is roughly 2.5%. The total cross-talk is about 15%. These figures take into account cross-talk from sense wires to one side only.

A program was therefore developed to calculate the signal propagation in multiwire chambers, by solving the telegraphers equation while taking into account the multiwire structure and electric properties of the chamber. With this tool it became possible to make a quantitative prediction of the amplitude of the cross-talk signal. This information was then used to develop a method for compensating the cross-talk. First the pulse shapes of real and cross-talk signals had to be equalized, which was achieved by a proper termination of the potential, cathode and sense wires. The second step was to cancel the cross-talk by a passive resistor network at the ouptut of the preamplifiers, which adds to each signal the appropriate amounts of the signals of the nearest and second nearest sense wires. The method and the calculations are described in detail in [12].

6.3 Performance of the chamber

To extract the timing information from the FADC-pulses, new algorithms have been developed. The Difference of Samples (DOS) scheme [13] proved to be the most versatile and the fastest method. It numerically differentiates the signal and calculates the weighted mean of the rising edge of the pulse. In addition it is able to resolve hits with small spatial separation. All the results presented here have been obtained with this method.

Fig. 10 shows the dependence of the spatial resolution on the drift distance. The deterioration due to increasing diffusion is much smaller than with conventional timing methods [14]. The average resolution of the

chamber is around 120 μm. For drift distances of a few centimeters the resolution is 80 μm, approaching the range previously covered by vertex detectors. One effect attributed to the cross-talk was the deterioration of resolution for tracks parallel to the anode plane. The measurements agree qualitatively with predictions from Monte-Carlo simulations of the drift process [15].

In order to make use of the good spatial resolution, systematic errors have to be small. Distortions of the drift field have been searched for with the laser system. Fig. 11 shows the results of such a scan. For the outer sense wires, where the laser beam is close to the corner between the cathode plane and the barrel field shaping electrode, a field distortion becomes apparent when using the present voltage settings. The maximal deviation from a straight line is of about 500 μm. Inhomogeneities such as this are easily detected by the laser system and can be removed by optimizing the drift field voltages applied to the chamber. Residual distortions will be corrected by software.

The sagitta error was determined with particle tracks to be 45 μm at small drift distances and 60 μm at large drift distances. This error is to be compared to the sagitta of a particle with 100 GeV/c transverse momentum in the 0.4 T magnetic field of OPAL, which is 380 μm.

The double track resolution was studied with simulated double hits generated by superimposing two real single hits. The efficiency for finding the second hit as a function of the distance between hits is shown in Fig. 12. At a distance of 2 mm this efficiency has already reached 85%. The time measurement for the second hit is slightly worse than for the first hit, the effect being a degradation of less than 50 μm at 2 mm separation.

The z coordinate along the sense wires is measured by charge division. Since the dE/dx measurement requires low gas gain to minimize saturation effects and charge division requires high gas gain to increase the signal to noise ratio, a compromise in the operating point has to be

found. The current gas gain is optimized more for charge measurement than for z measurement, because in OPAL the jet chamber will be surrounded by a layer of chambers especially designed to measure the z-coordinate [1]. After calibration with tracks of known position in z, a resolution of about 4 cm has been achieved (Fig. 13).

An important design goal for the OPAL jet chamber is the measurement of the specific energy loss of particles with a resolution of 3 to 4%. First results from the beam run in 1984 demonstrated that this could be achieved, matching the specifications of the technical proposal. However, the data indicated that the particle separation was slightly worse than expected from JADE measurements [16]. This was attributed to angle and amplitude dependent saturation effects. Therefore in the beam tests of May 1985 the gas gain was reduced by a factor of two. Since at that time a modification of the electronics gain was not possible, threshold effects had to be taken into account. Fig. 14 shows that the energy ratio E_e/E_π for electrons and pions at 6 GeV is now very close to expectation. Fig. 15 demonstrates the particle separation power of the FSP; the peaks in the specific energy loss for electrons, pions and protons are clearly separated. Averaged over the angle between the track and the normal to the sense wires from 0 to 20 degree, the π/e separation $(E_e - E_\pi)/\sigma_\pi$ is 3.7.

In 1986 another beam test will be performed to further optimize the operating conditions. The improvements introduced for this test include an increased gain of the preamplifiers and cross-talk compensation for both sectors of the FSP.

7. CONCLUSIONS

The full scale prototype of the OPAL jet chamber has worked reliably for nearly two years. All basic goals have been achieved: the design of the jet chamber has been demonstrated to be sound, important components like the field shaping and the high voltage insulation, the HV supply and safety system, the gas purification system, the FADC readout and the laser calibration

have been shown to work at the scale of the final OPAL detector. Finally, it has been demonstrated that the resolution of the chamber is in all respects as good as, or better than expected.

Valuable experience is being gained in the development of analysis procedures for extracting time and charge information from the recorded pulse forms. The FSP is at present being used to test new or improved components and to refine the operating parameters of the chamber. The experience gained with this device continues to influence the design and manufacturing of the final chamber for OPAL.

ACKNOWLEDGEMENT

The design, construction and assembly of this full scale prototype would not have been possible without the enthusiastic help from many persons. We would like to thank A. Beer, W. Bichler, L. Briot, G. Chil, G. Critin, G. Lamoureux, G. Linser, R. Lorenzi, and P. Loup at CERN; H. Ganter, G. Heine, G. Tautz and N. Wilfert at the Freiburg University; and E. Bernauer, E. Ehrbar, J. Gerhäuser, S. Hennenberger, K. Hoke, R. Hotz and Ch. Rummel at the Heidelberg University.

D. Plane looked after the test beam and the measurements were performed with the help of J. Engelfried, M. Huk, T. Kunst, W. Leibold and A. Michels.

B. Schmidt, Heidelberg, has measured the influence of water on the drift velocity and has advised us in many questions regarding the choice of gas.

We would also like to thank the OPAL Saclay group which provided us with an efficient microprocessor based data acquisition system.

This work was supported in part by the Bundesministerium für Forschung und Technologie.

Table 1

Preamplifier VV36	
Type	Common base input, differential output
Input impedance	40 Ohm
Gain (at 100 Ohm)	100
Rise and fall time response	about 6 nsec
Noise	about 2000 electrons r.m.s.

Table 2

Flash ADC DL300	
Gain of differential receiver	10
FADC chip	Siemens SDA 5010
Sampling frequency	100 MHz
Dynamic range	6 bit, extended to about 8, bit non-linear
Memory depth	256 samples, now extended to 1024 samples

REFERENCES

[1] The OPAL Detector Technical Proposal; CERN/LEPC/83-4, LEPC/P3

[2] H. Drumm et al., Nucl. Instr. and Meth. 176 (1980), 333.

[3] W. Farr et al., Nucl. Instr. and Meth. 156 (1978), 283.

[4] H.J. Burckhart et al., CERN EF/85-11, Submitted to Nucl. Instr. and Meth.

[5] Silver solder ERSIN Multicore

[6] Wire tension meter, type NE-660, made in Hungary (KFKI).

[7] B. Schmidt, paper presented at the IV Vienna Wire Chamber Conference.

[8] M. Huk, Diploma Thesis, Physik Institut Univ. Heidelberg 1986.

[9] P.V. Walter, G. Mildner, IEEE Trans. Nucl. Sci. NS-32 (1985), 626.

[10] K.W.D. Ledingham et al., Nucl. Instr. and Meth. A241 (1985), 441.
A. Bamberger et al., CERN-EP/85-182, Submitted to Nucl. Instr. and Meth.
J.W. Cahill et al., CERN-EP/85-182, Submitted to Journ. of Physics B
S.L.T. Dysdale et al., Dept. of Nat. Phi.; Univ. of Glasgow.

[11] L. Stieglitz, Kernforschungsanlage Karlsruhe, private communication.

[12] P. Bock et al. presented at the IV Vienna Wire Chamber Conference, to be published.

[13] D. Schaile et al., Nucl. Instr. and Meth. A242 (1986), 247.

[14] W. Farr et al., IEEE Trans. Nucl. Sci NS-30 (1983), 95.
P. Bock et al., Nucl. Instr. and Meth. A242 (1986) 237.

[15] H.J. Mayer, to be published.

[16] Jade group, private communication.
I. Lehraus, Nucl. Instr. and Meth. 217 (1983), 43.

FIGURES CAPTIONS

Fig. 1 Cut through one quadrant of the final OPAL jet chamber in a plane perpendicular to the beam axis and a view along the beam. The cathode and sense wire planes, the conical endplate (1), the shell of aluminium panels (2), barrel (3) and endcap (4) field shaping electrodes, the inner field shaping (5), the anode wire suspension (6) and the z-chambers (7) are indicated.

Fig. 2 Cross section of the OPAL jet chamber full scale prototype

Fig. 3 Cross section through one half sector of the jet chamber showing details of the cathode and sense wire planes. Also indicated are the barrel (1) and endcap (2) field shaping electrodes.

Fig. 4 Mounting scheme of anode, potential and cathode wires to the endplate. The main components of the anode wire suspension besides the mechanical fixations are a comb like structure (1) for the precise positioning of the wires, the printed circuit boards equipped with solder pads and pins (2) to hold the wires and the preamplifiers (3). The blow-up of the anode comb shows the two rows of grooves for positioning of the potential and sense wires. Note the different depths of the grooves to achieve the staggering of the sense wires.

Fig. 5 Cut away view of the structure serving as support for the cathode wires and as field shaping electrode. The front part consists of the wire suspension, the wire positioning comb, one PC board holding the wires and the resistor chain and another PC board with the field electrodes. The back part consists of the field degrader and an aluminium profile.

Fig. 6 Wire positioning accuracy in the anode plane.

Fig. 7 Schematic layout of the high voltage system.

Fig. 8 Layout of the gas system:
(1) Heatable molecular sieve saturated with water,
(2) FSP pressure vessel (30 m^3),
(3) Small test chamber,
(4) High-precision manometer
(5) Compressors (6 m^3/h and 3 m^3/h) for gas circulation,
(6) Teledyne trace oxygen analyzer,
(7) Activated copper filter (BASF-R311),
(8) Shaw hygrometer,
(9) Molecular sieve (3 A cell size),
(10) Filter.
Valves to select the desired flow path and visual flowmeters are also indicated. The arrows indicate the direction of the gas flow.

Fig. 9 Schematic layout of the laser calibration system. The distance of the two laser beams in drift direction is 10 mm.

Fig. 10 Timing accuracy σ as function of drift distance for various angles of the particle beam with respect to the anode plane (φ = 0 corresponds to tracks parallel to the anode plane).

Fig. 11 Field distortions detected by the laser system. The distortion occurs at the outer corner of the drift cell where the cathode plane and the barrel field electrode meet.

Fig. 12 Efficiency of double hit resolution as a function of hit separation.

Fig. 13 Accuracy σ_z for the determination of the coordinate along the wire (z).

Fig. 14 Energy loss ratios for electrons, pions and protons at 6 GeV/c as a function of the angle between the beam and the sense wire. The dashed lines represent the expectation for E_e/E_π and E_e/E_p.

Fig. 15 Energy loss distribution for protons, pions and electrons at 6 GeV/c.

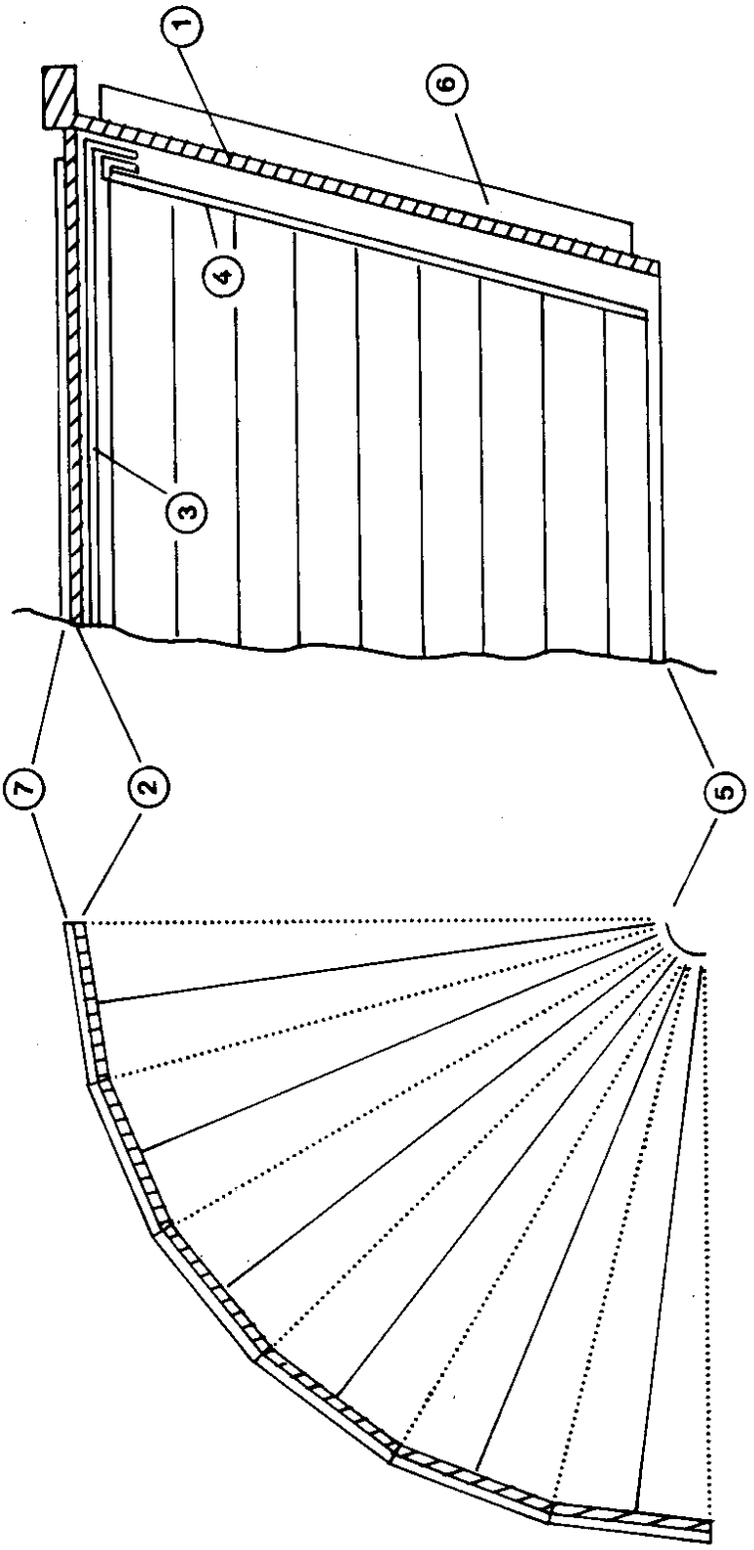

FIG. 1

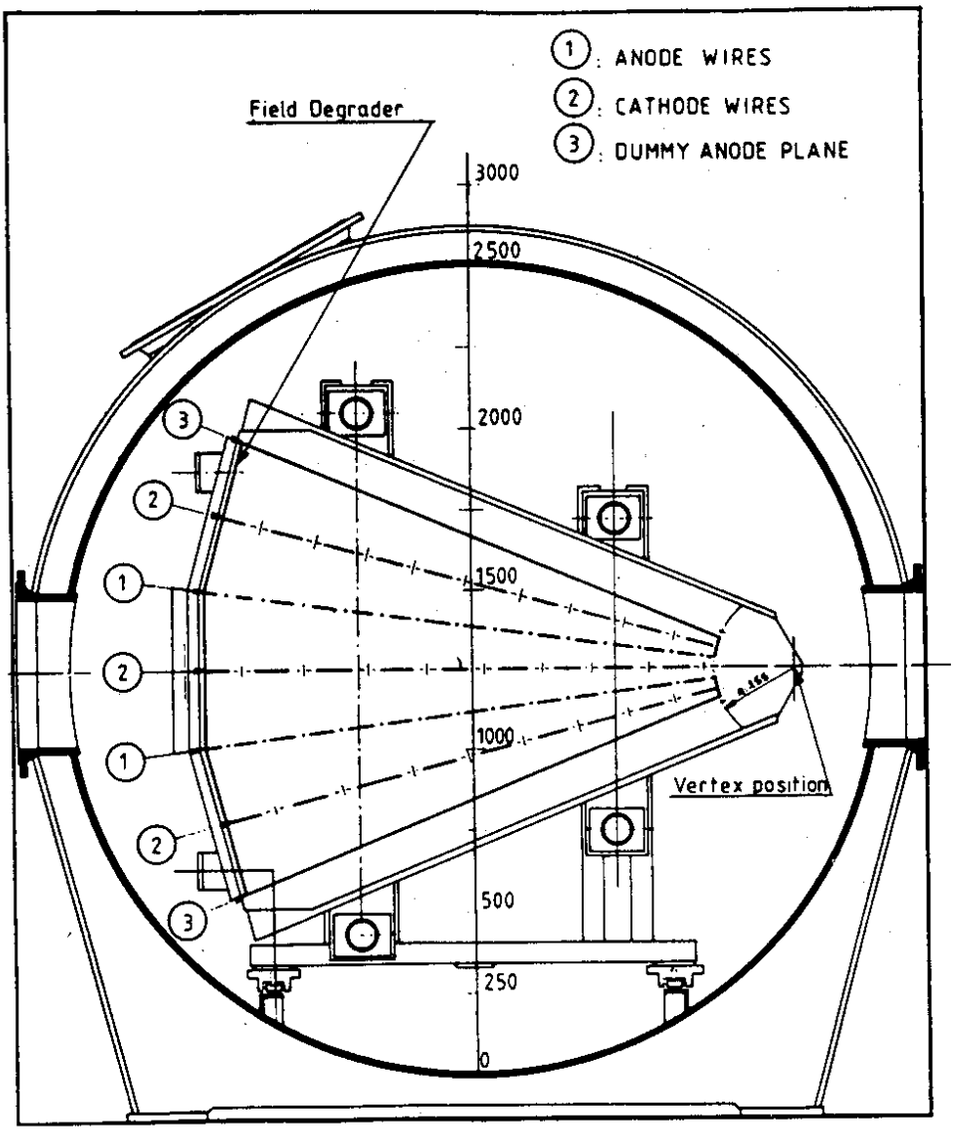
1 : ANODE WIRES
2 : CATHODE WIRES
3 : DUMMY ANODE PLANE
Field Degrader
3000
2500
2000
1500
1000
500
250
0
Vertex position

FIG. 2

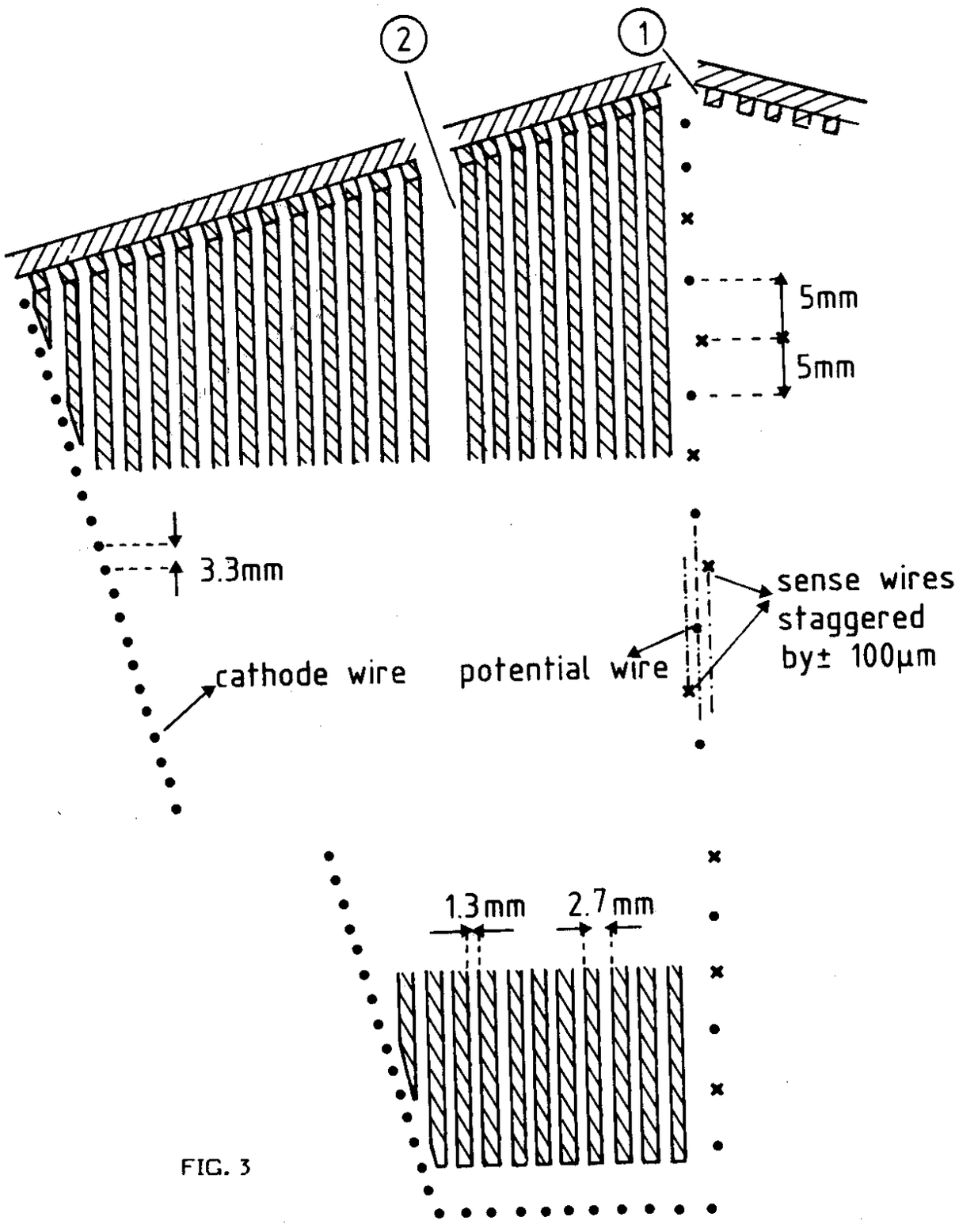
2
1
5mm
5mm
3.3mm
cathode wire
potential wire
sense wires
staggered
by± 100µm
1.3mm
2.7mm

FIG. 3

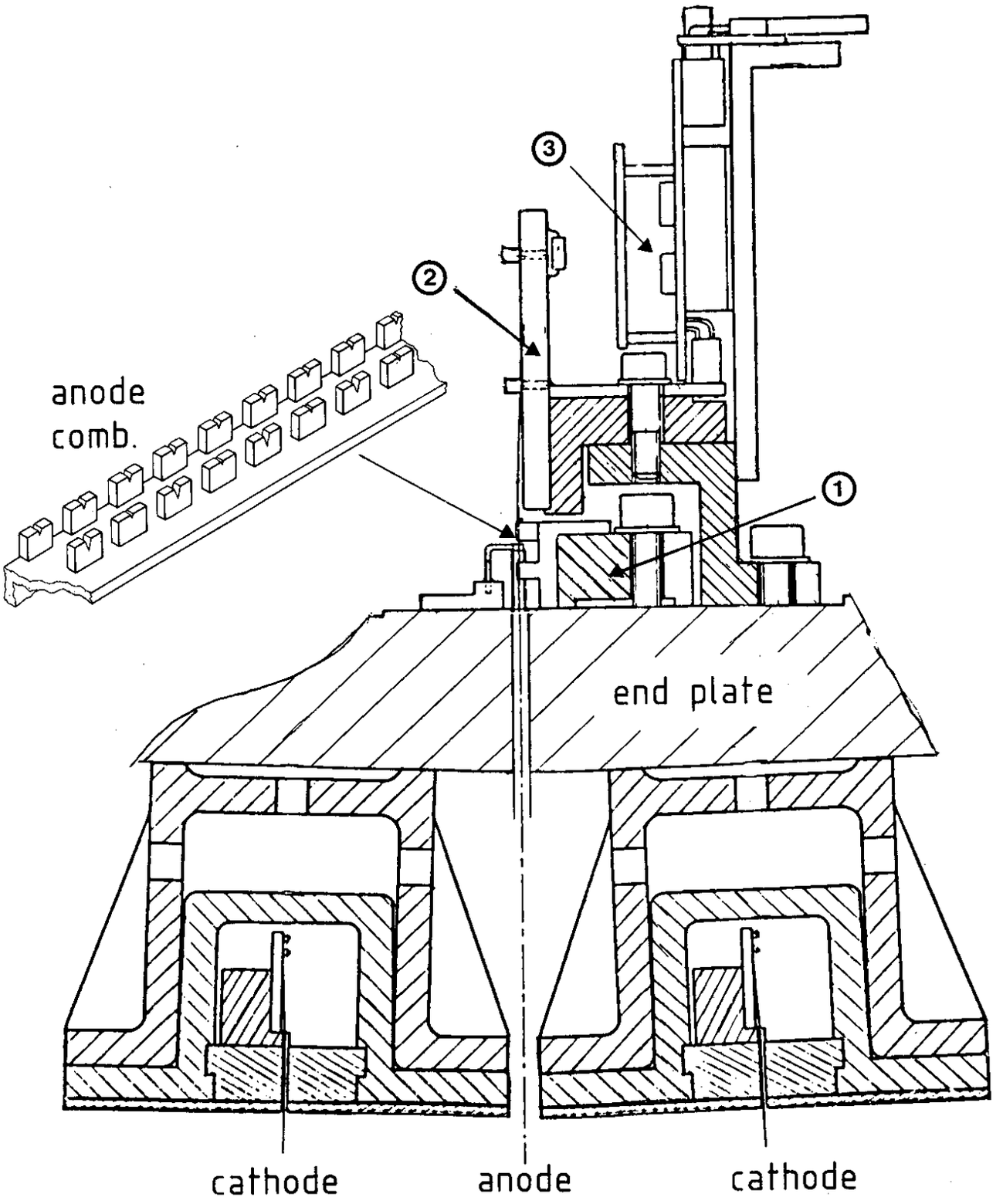

FIG. 4

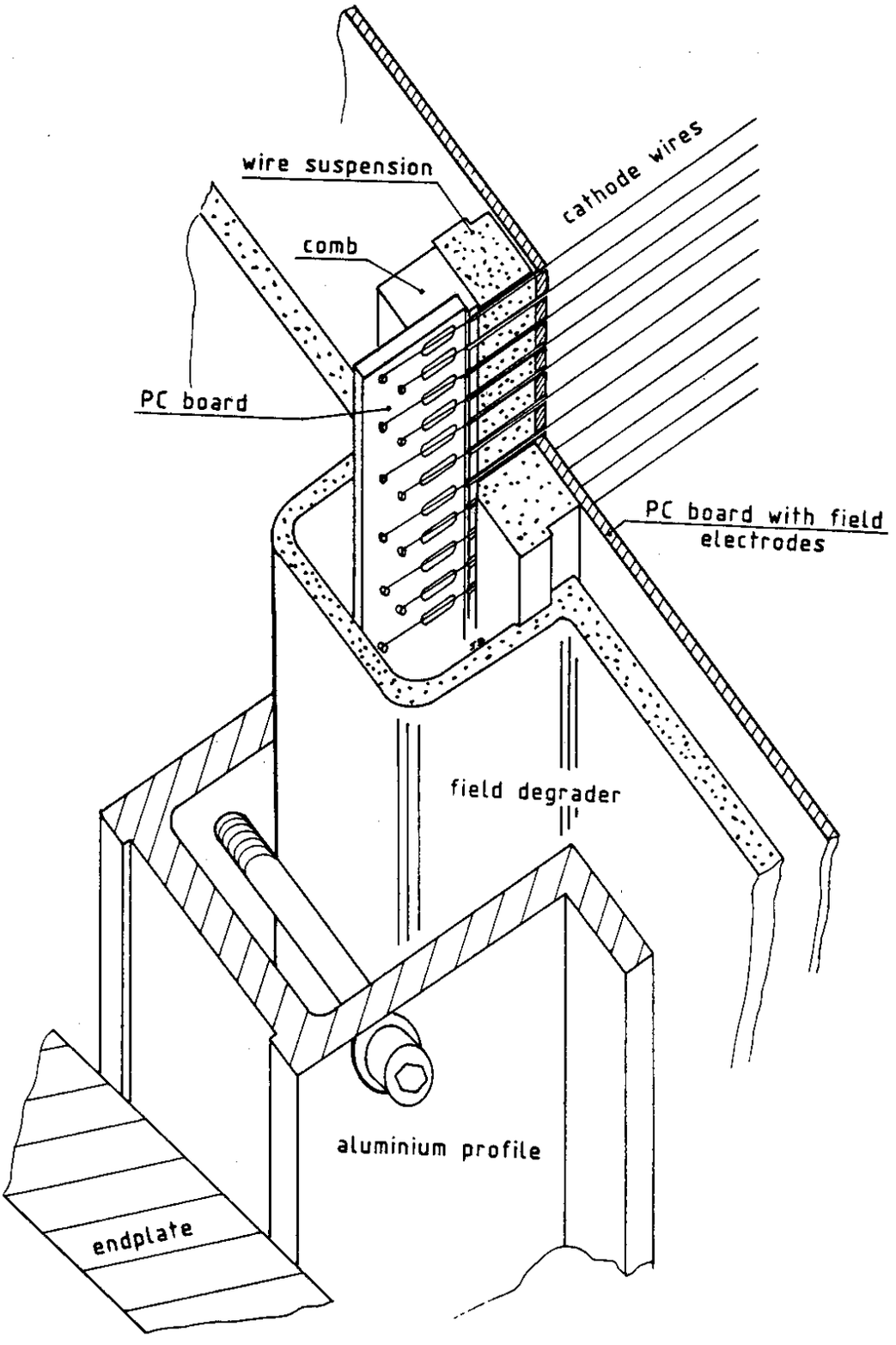
wire suspension
cathode wires
comb
PC board
PC board with field electrodes
field degrader
aluminium profile
endplate

FIG. 5

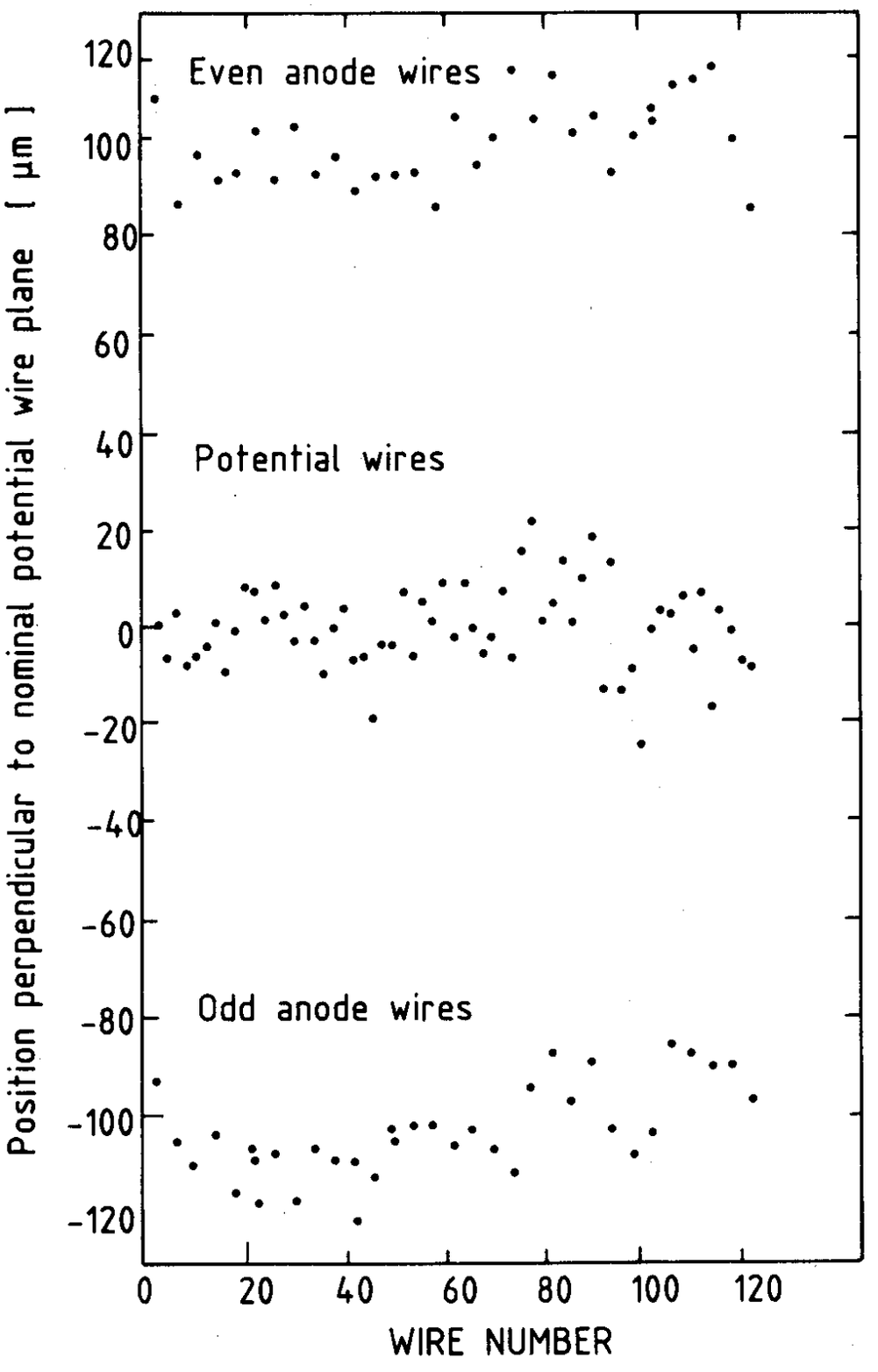
Even anode wires
Potential wires
Odd anode wires
Position perpendicular to nominal potential wire plane [µm]
WIRE NUMBER
120
100
80
60
40
20
0
-20
-40
-60
-80
-100
-120
0
20
40
60
80
100
120

FIG. 6

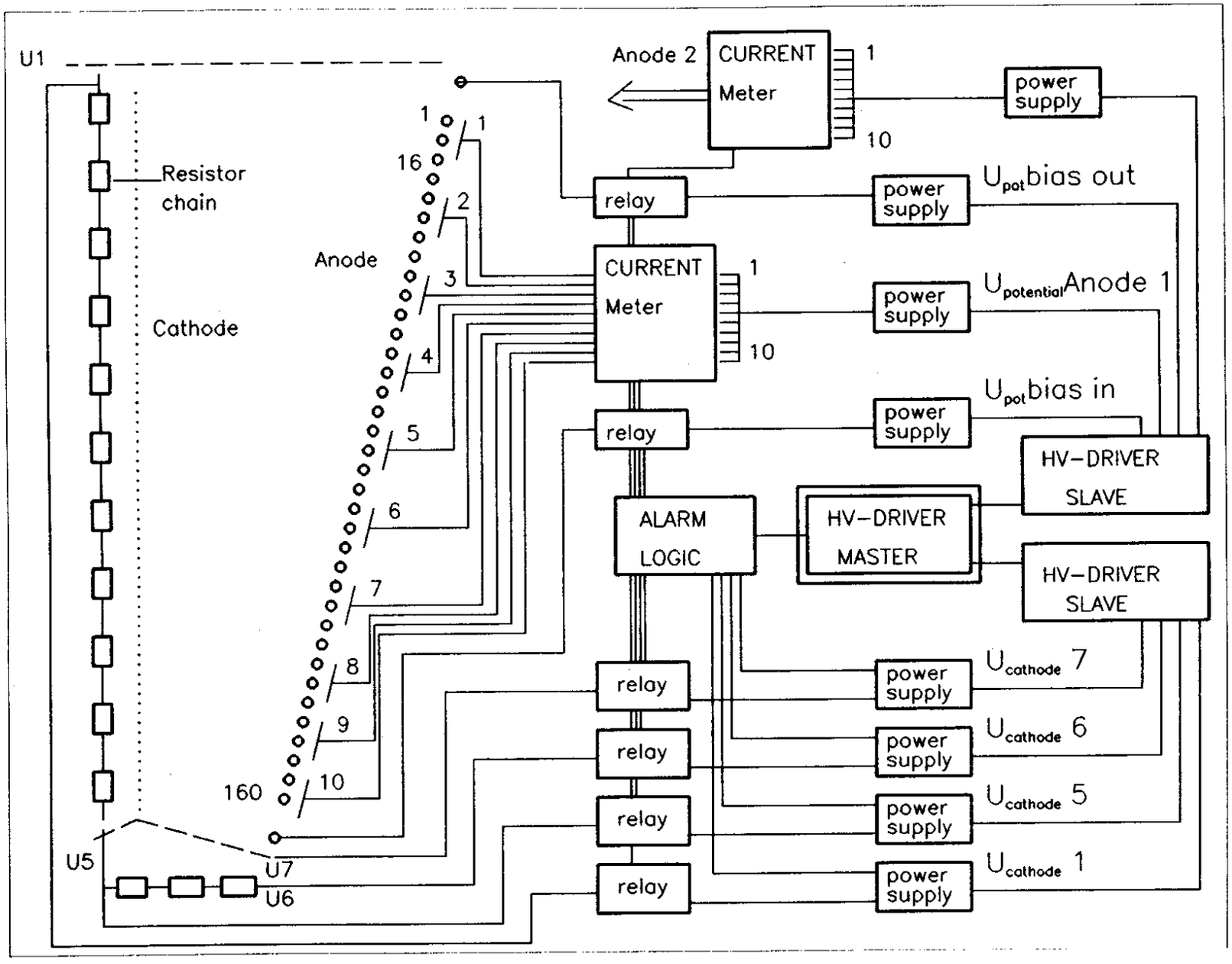
U1
Resistor chain
Cathode
Anode
1
16
2
3
4
5
6
7
8
9
160
10
U5
U7
U6
Anode 2
CURRENT Meter
1
10
power supply
relay
power supply
U_{pot} bias out
CURRENT Meter
1
10
power supply
$U_{potential}$ Anode 1
relay
power supply
U_{pot} bias in
HV–DRIVER SLAVE
ALARM LOGIC
HV–DRIVER MASTER
HV–DRIVER SLAVE
relay
power supply
$U_{cathode}$ 7
relay
power supply
$U_{cathode}$ 6
relay
power supply
$U_{cathode}$ 5
relay
power supply
$U_{cathode}$ 1

FIG. 7

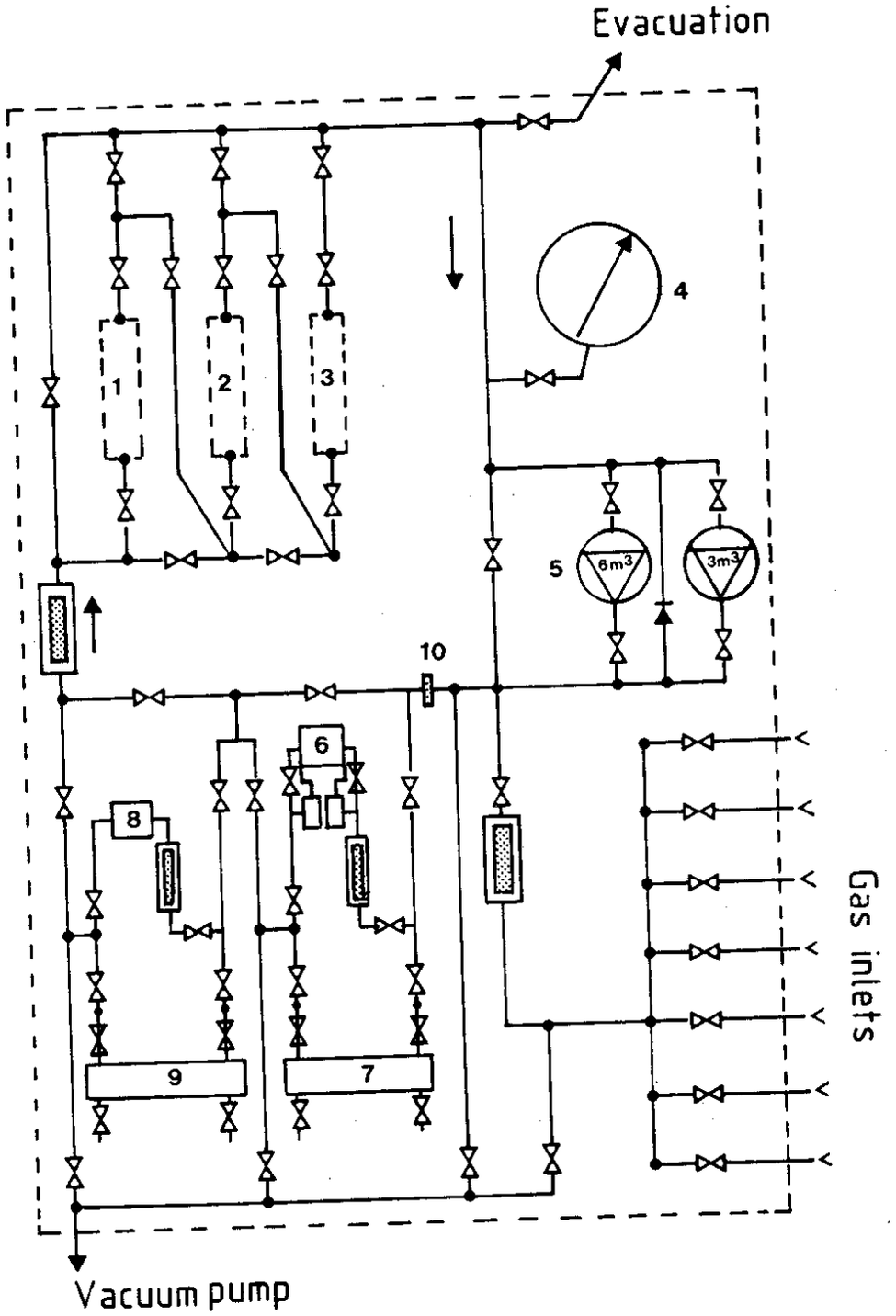

FIG. 8

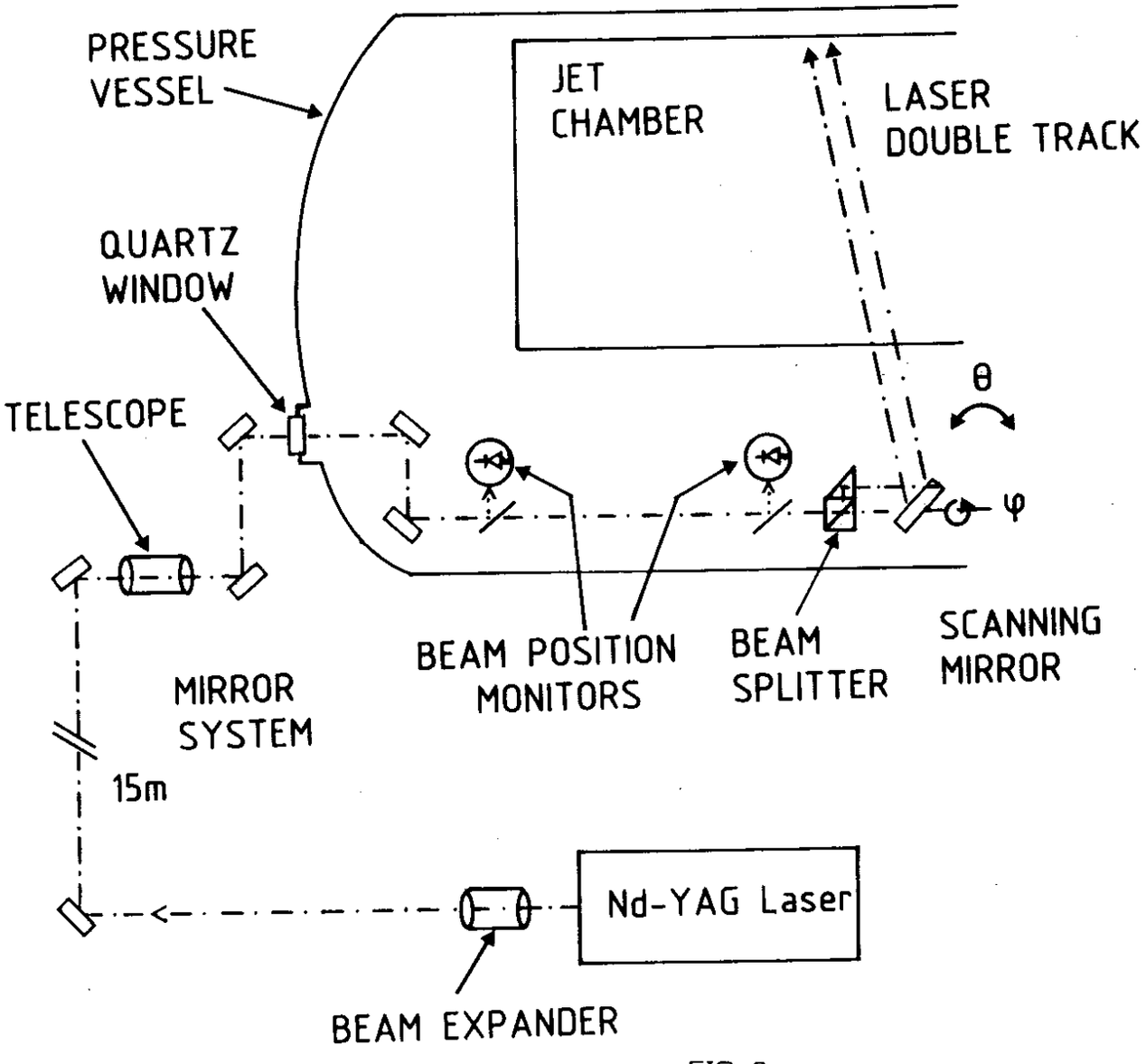
PRESSURE
VESSEL
JET
CHAMBER
LASER
DOUBLE TRACK
QUARTZ
WINDOW
θ
TELESCOPE
φ
BEAM POSITION
MONITORS
BEAM
SPLITTER
SCANNING
MIRROR
MIRROR
SYSTEM
15m
Nd-YAG Laser
BEAM EXPANDER

FIG. 9

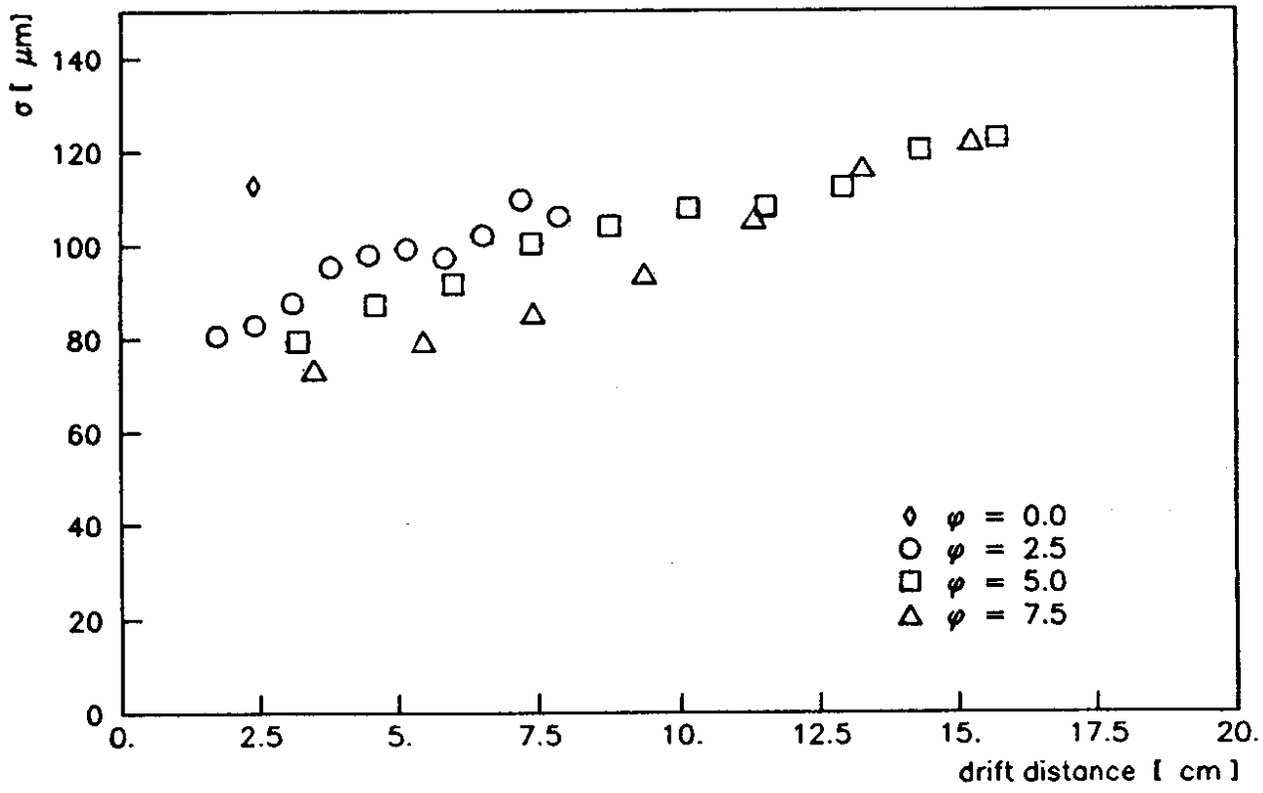
σ [μm]
140
120
100
80
60
40
20
0
0.
2.5
5.
7.5
10.
12.5
15.
17.5
20.
drift distance [cm]
◊ φ = 0.0
○ φ = 2.5
□ φ = 5.0
△ φ = 7.5

FIG. 10

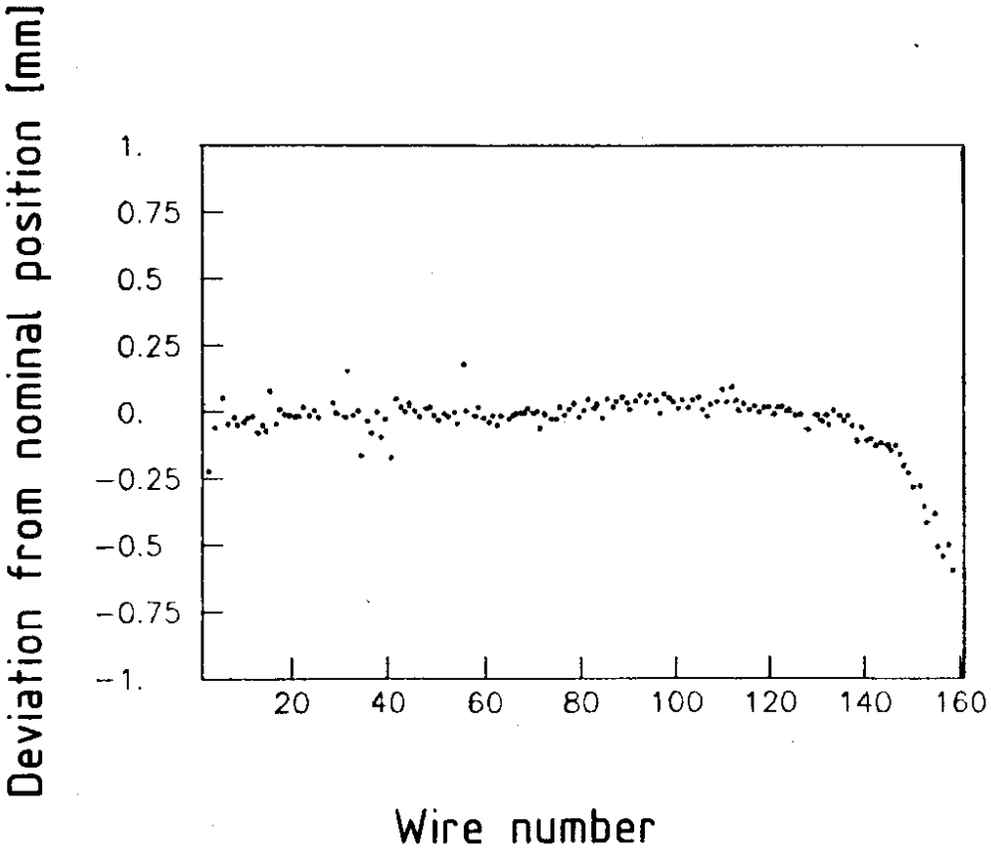
Deviation from nominal position [mm]
1.
0.75
0.5
0.25
0.
−0.25
−0.5
−0.75
−1.
20
40
60
80
100
120
140
160
Wire number

FIG. 11

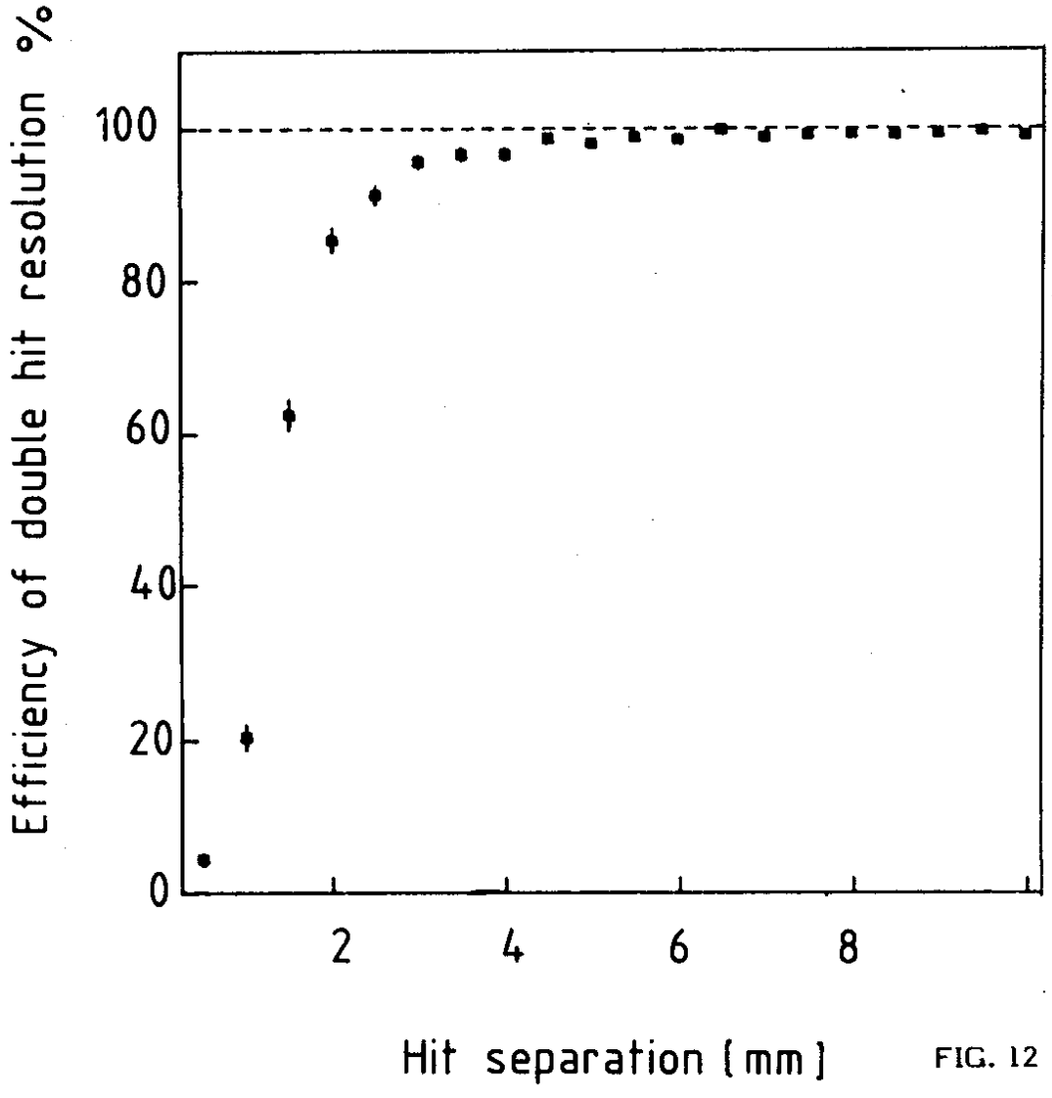
Efficiency of double hit resolution %
100
80
60
40
20
0
2
4
6
8
Hit separation [mm]

FIG. 12

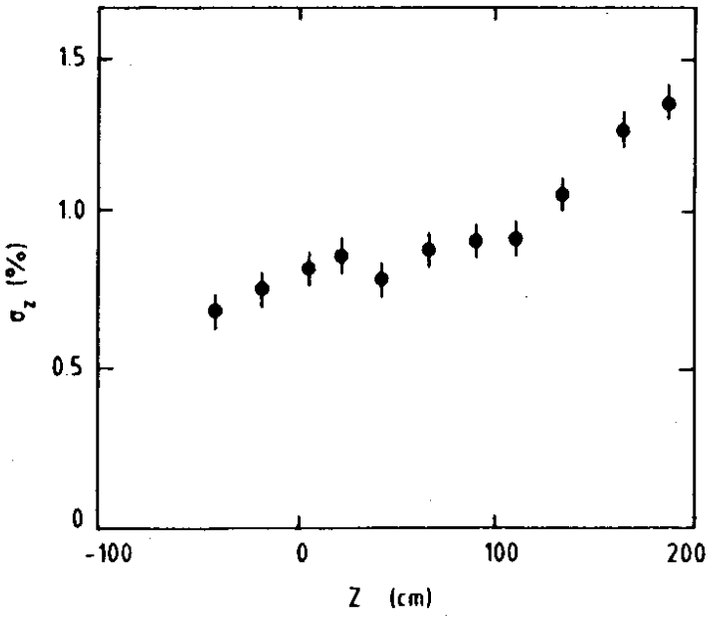

FIG. 13

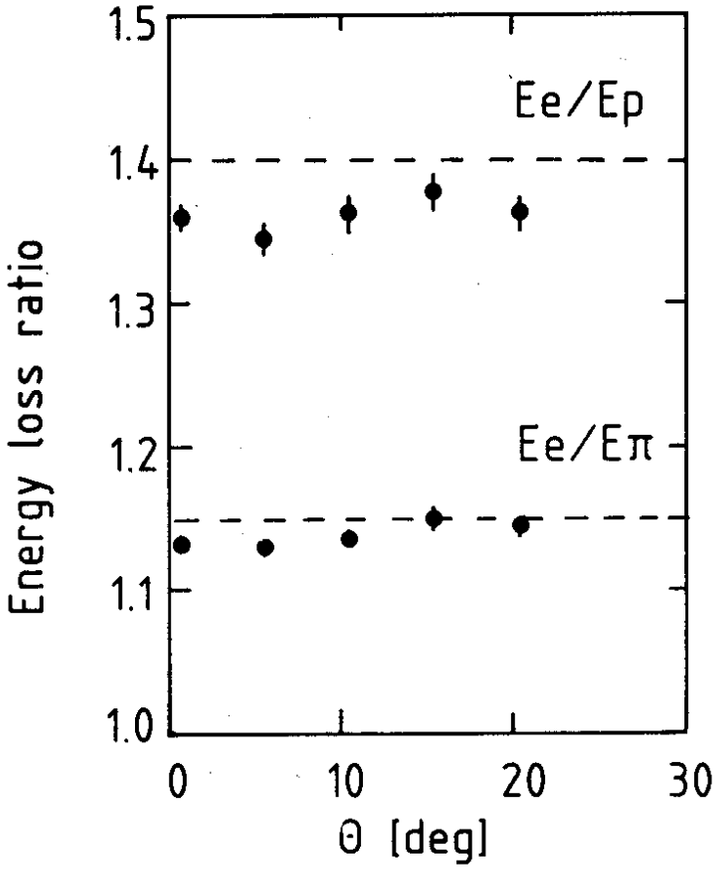

FIG. 14

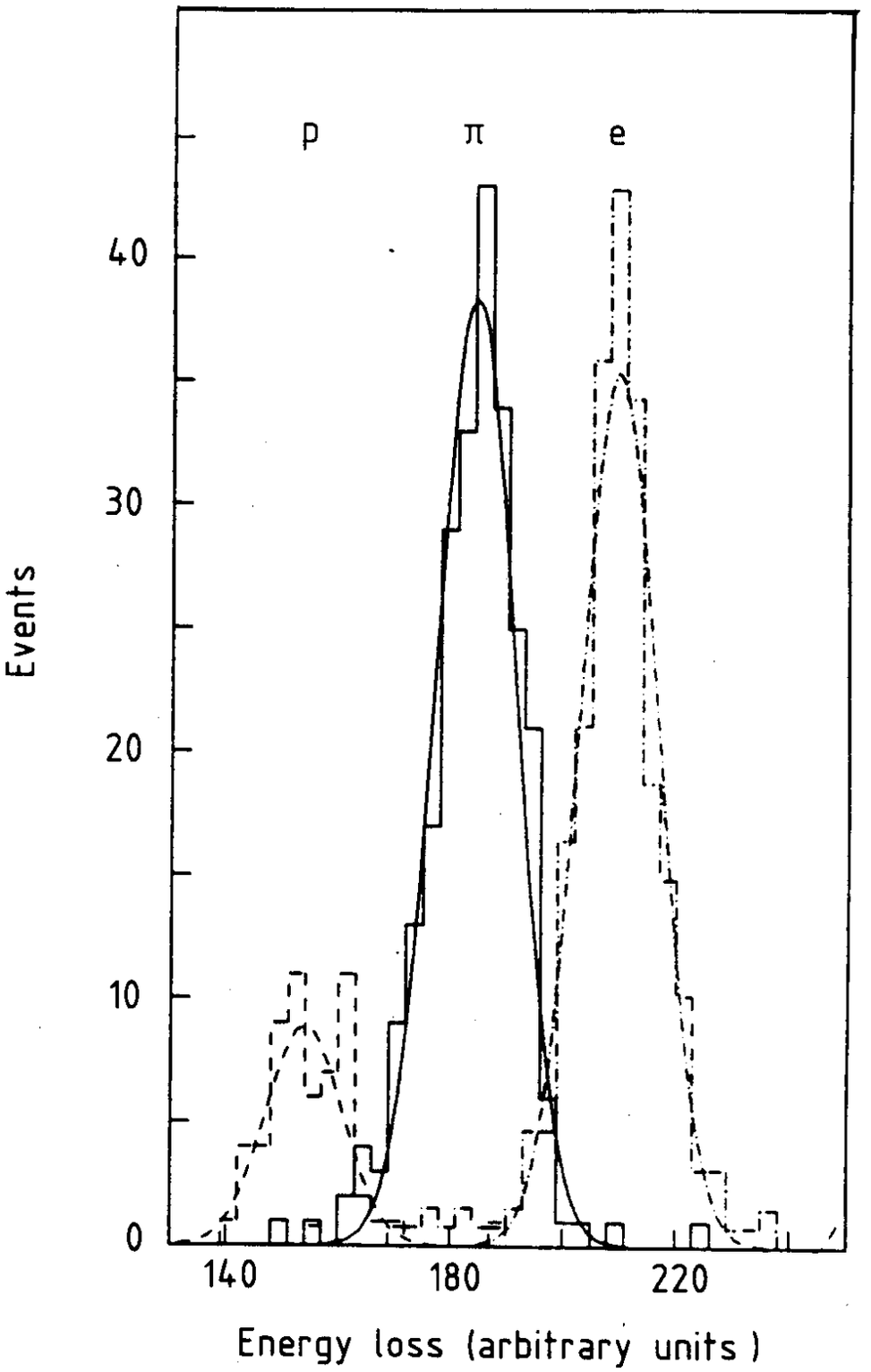
p
π
e
40
30
20
10
0
Events
140
180
220
Energy loss (arbitrary units)

FIG. 15